PAPER

Check for updates

Interface-enhanced CO_2 capture *via* the synthetic effects of a nanomaterial-supported ionic liquid thin film†

Yang Liu, [ID] [a] Yanmei Yang, [ID] *[b] Yuanyuan Qu, [ID] [a] Yong-Qiang Li, [ID] [a] Mingwen Zhao [ID] [a] and Weifeng Li [ID] *[a]

Ionic liquids (ILs) are effective CO_2 capture media and recent experimental evidence has demonstrated that the addition of two-dimensional (2D) nanomaterials into ILs can effectively improve their CO_2 capturing capability. However, an in-depth mechanism on how 2D nanomaterials enhance CO_2 absorption is poorly documented. In this study, the adsorption of CO_2 by a representative IL, namely 1-ethyl-3-methyl-imidazole-tetrafluoroborate ([EMIM][BF_4]), coated on graphene (GRA, the prototype 2D nanomaterial) and nitrogenized graphene (C_3N) was investigated by molecular dynamics simulations. The influence of the IL film thickness on the amount of CO_2 adsorption was systematically analyzed. Our data clearly indicate that at the IL-gas interface the CO_2 accumulation is significantly enhanced. In contrast, at the IL-GRA and IL-C_3N interfaces, only slight enhancement was observed for CO_2 accumulation. Quantitative calculations of the adsorption-free energy for CO_2 inside the IL film further support the simulation results. Our present results also reveal that the sub-nanometer IL film possesses a considerably high CO_2 capture efficiency because of the formation of the reduced bulk IL region. Moreover, the nanomaterial substrate surfaces can effectively accelerate the diffusion of CO_2, which is beneficial for the CO_2 mass transfer. In general, our theoretical study provides a deep microscopic understanding of the CO_2 capture by nanomaterials and IL composites. These results could benefit the design and fabrication of a high-performance CO_2 capture and storage medium through the synthetic effects of ILs and nanomaterials.

1. Introduction

To slow the pace of global warming, considerable efforts have been made towards the development of novel strategies for mitigating CO_2 emission, particularly for the CO_2 capture and sequestration (CCS) in the past two decades.[1,2] Among numerous materials under study, ionic liquids (ILs) have received remarkable attention from both industry and academia since the first report of using ILs in CCS.[3] The outstanding capability of ILs to attract CO_2 lies in their unique physical and chemical properties including the high affinity towards CO_2, the vanishingly low vapor pressure, the high thermal and chemical stability and the low energy consumption for regeneration.[4–6] Benefitting from these distinguished

features, ILs are widely accepted as promising candidates for being economic and environmental-friendly capture-medium for CO_2. More importantly, the advantages of ILs are reflected in the abundant types of the composed cations and anions in ILs. Thus, the properties of ILs can be customized to match different CCS requirements.[7]

Despite the high performance of ILs for CO_2 capture, severe drawbacks still exist, which hinder their industrial usage. In particular, the high viscosity induced by the hydrogen-bond network inside ILs unavoidably slows down the kinetic speed for CO_2 uptake and separation.[8] In addition, it is also reported that the absorption of CO_2 can in turn increase the viscosity of ILs.[9] To overcome this drawback, one solution is building supported IL membranes (SILMs) by coating ILs on the surface of solid materials.[10,11] In previous studies, researchers found that the thickness of IL films is a key factor to attract CO_2. Earlier experiments have shown that when the thickness of an IL membrane decreases from the microscale to nanoscale, the CO_2 mass transfer rate has a hundred-fold increase.[12] This, according to the diffusion-reaction theory,[13] is because the diffusion-controlled process in the thick layer is switched to the surface-reaction controlled process when IL thickness decreases. It is also reported that the thin IL film on the

[a]School of Physics, State Key Laboratory of Crystal Materials, Shandong University, Jinan, Shandong, 250100, China. E-mail: lwf@sdu.edu.cn

[b]College of Chemistry, Chemical Engineering and Materials Science, Collaborative Innovation Center of Functionalized Probes for Chemical Imaging in Universities of Shandong, Key Laboratory of Molecular and Nano Probes, Ministry of Education, Shandong Normal University, Jinan, 250014, China. E-mail: yym@sdnu.edu.cn

† Electronic supplementary information (ESI) available. See DOI: 10.1039/d0na00875c

substrate can enhance the confinement effect, which accelerates its diffusion and the adsorption of CO_2.[14,15] Despite these previous studies, the molecular mechanism of how IL molecules interact with the CO_2 gas in the confined space is still poorly documented, which becomes the main hindrance for further experimental research.

Here, molecular dynamics (MD) simulations have been conducted to explore the molecular mechanism of SILM for CO_2 capture. The commonly used 1-ethyl-3-methyl-imidazole-tetrafluoroborate [EMIM][BF_4] was used as the representing IL model. However, for nanomaterial substrates, we choose graphene (GRA, a prototype 2D nanomaterial) and C_3N (a recently synthesized 2D structure,[16] which was used for controllable CO_2 capture and release[17–19]), as representative models. The influence of the IL film of various thicknesses in CO_2 capturing was systematically addressed.

Our results clearly indicate that the GRA/C_3N substrates introduced two interfacial faces in the IL film, the substrate-IL interface and IL-gas interface, with distinct IL ordering structures compared to that in the bulk IL. The CO_2 capturing efficiency of the supported IL increases with a decrease in the IL film thickness. Among two interfacial regions, the clear accumulation of CO_2 is found at the IL-gas interface region, which plays a key role in enhancing the CO_2 capturing capability than that with bulk IL. In contrast, the substrate-IL interfacial region plays a minor role in CO_2 capture. However, the substrate-IL interface is beneficial for the diffusion of IL and CO_2, particularly for graphene, which is beneficial for the CO_2 mass transfer. More importantly, our results also reveal that the sub-nanometer IL film possesses a significantly higher CO_2 capture efficiency because of the formation of a reduced bulk IL region. Our present findings provide a deep understanding of the interactions between the SILM components with CO_2, which are important to guide the design and optimization of SILMs for the CCS usage.

2. Simulation methods

2.1 Model setup

The GRA nanosheet has a dimension of 2.993×3.455 nm^2 and is composed of 392 carbon atoms. The C_3N nanosheet has a dimension of 3.104×3.584 nm^2 and is composed of 96 nitrogen and 288 carbon atoms. Previous studies have shown that compared to the monolayer substrate the multilayer substrates can affect the adsorption of molecules in a limited manner.[20] Thus, in our simulation, we only focused on the monolayer substrate. The nanosheet is placed parallel to the x–y plane of the simulation box and the cross-section of the simulation box is equal to the size of the nanosheet. A space of 10 nm is placed along the z direction. Five systems with different numbers of [EMIM][BF_4], which were 20, 50, 80, 110 and 140, coated on the surfaces of GRA and C_3N were prepared, respectively. The thickness of the IL film was estimated from the 2D layer to the IL-gas interface with the IL density being half of the bulk value. After equilibration of 10 ns, the IL film thicknesses were estimated to be 0.57 nm, 1.57 nm, 2.41 nm, 3.26 nm and 4.09 nm for the five GRA systems, and 0.57 nm, 1.43 nm,

2.21 nm, 3.00 nm and 3.76 nm for the five C_3N systems, as demonstrated in Fig. S1 in the ESI.† Then, 200 CO_2 molecules were randomly added to the vacuum region of each system, as depicted in Fig. 1c and d.

2.2 Simulation parameters

All MD simulations were performed using the GROMACS 5.1.3 package.[21] The force field parameters for [EMIM][BF_4],[22] CO_2,[13] and C_3N[23] were adopted from previous studies in which they were optimized by precise quantum chemistry calculations. During the simulation, a leap-frog algorithm was used to integrate the Newton equations of motion, and the time step was set to 1 fs. All bonds involving hydrogen atoms were constrained using the LINCS algorithm.[24] All the atoms in GRA/C_3N were position-restrained to maintain a planar surface during the whole simulation. The cutoff for both the electrostatic and van der Waals (vdW) interactions was 1.0 nm. Long-range electrostatic interactions were calculated using the particle mesh Ewald (PME) method.[25] All the simulations were performed under the NVT ensemble, where the V-rescale algorithm[26] was applied to the system to maintain a constant temperature of 298 K. Totally 200 ns production trajectory for each system was collected for CO_2 molecules to dissolve into the IL film, and the last 30 ns trajectories were used for the data analysis.

2.3 Quantitative interpretation of the CO_2-binding affinity by umbrella sampling

To quantitatively evaluate the binding affinity of CO_2 by the IL film, the potential of mean force (PMF) of a single CO_2 molecule diffusing from the IL-gas interface into the substrate-IL interface was quantitatively calculated *via* the umbrella-sampling method.[27–29] The separation between CO_2 and the nanosheet is selected as a collective variable (CV). Totally 20 points were sampled along with the CV. The harmonic force with a constant of 1000 kJ mol^{-1}·nm^{-2} was applied to the CO_2 molecule. Each point was sampled for 10 ns, and the PMF profile was generated using the Weighted Histogram Analysis Method.[28]

3. Results and discussion

3.1 IL distributions on the substrate

To investigate the role of GRA and C_3N substrates on the IL film, we first characterized the structural features of the IL film on the two substrates. Fig. 2a–d depict the number density profiles of cation [EMIM]$^+$ and ion [BF_4]$^-$ along the normal direction of GRA and C_3N, respectively. Except for the system with an IL thickness of 0.57 nm, two clear peaks, which represented the first and second binding shells of cations (Fig. 2a and b) and anions (Fig. 2c and d) around the substrate, were detected. The high value indicates a strong attraction of the substrate towards IL molecules. Such phenomenon agrees well with the previous reports about the 2D material and IL interaction.[14,30] Beyond these two peaks, the density profiles of the ions reach a plateau with only slight fluctuation, until they drop to zero when being far away from the nanosheets. Based on the variation of the density profiles of ILs, the IL film is divided into three regions:
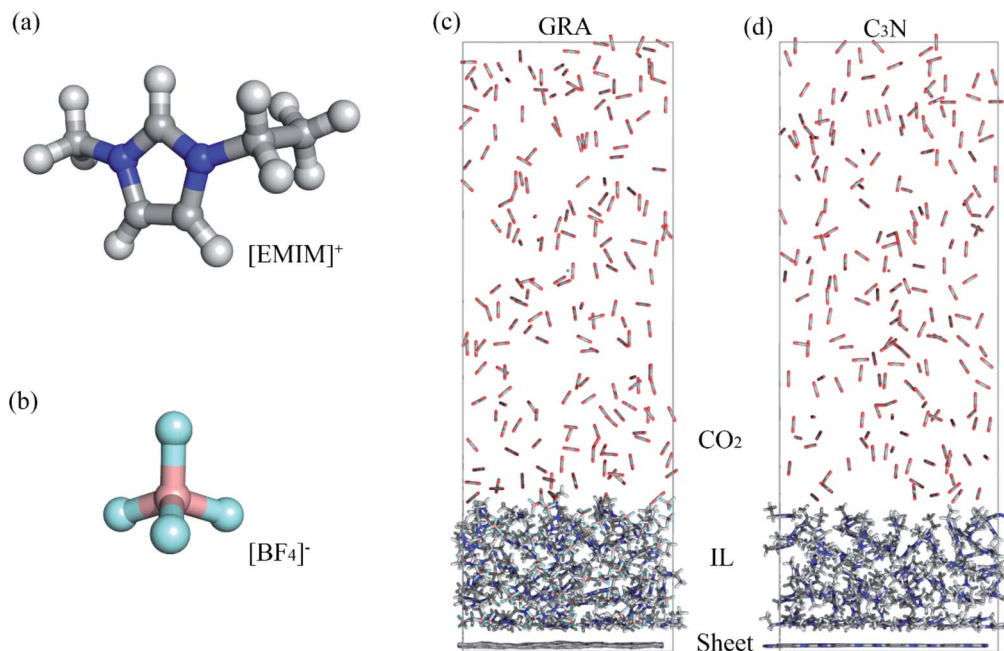
Fig. 1 Structures of cation $[EMIM]^+$ (a) and anion $[BF_4]^-$ (b), and schematic representations of the simulation box for IL coated on GRA (c) and C_3N (d).

(1) the substrate-IL interfacial region that covers the first two binding shell of IL, (2) the bulk IL region where IL is evenly distributed, and (3) the IL-gas interfacial region where the IL density starts to diminish. For the three regions, the thicknesses of the two interfacial regions are relatively constant, except that the bulk IL region varies in different systems. In the extreme case of the IL film with a thickness of only 0.57 nm (the black lines in Fig. 2a–d), the substrate-IL and IL-gas interfacial regions merge without the bulk IL region.

3.2 The CO_2 assembly in the IL film

The CO_2 molecules were initially placed outside the IL film. During the simulations, varying number of CO_2 molecules adsorbed and intruded into the IL film. Fig. 2e and f depict the number density profiles of CO_2 along the normal direction of

GRA and C_3N. For each system, there are two detectable CO_2 peaks at the substrate-IL interface, which represent the direct attraction of GRA and C_3N towards CO_2. In addition, one dominant peak can be detected for the density profile, which was located at the edges of the IL film, particularly, at the IL-gas interface. When the thickness of the IL film decreases, this peak shifts according to the IL-gas interface. For the thinnest IL film with a thickness of 0.57 nm, the two accumulative regions of CO_2 merge into one. More importantly, CO_2 accumulation inside a 0.57 nm IL film is significantly enhanced than that in other systems, as indicated by the highest peak among the five systems. This reflects synergistic effects from both the substrate-IL and IL-gas interfaces in the thinnest IL film. Moreover, the CO_2 densities in the bulk IL regions are found to be constant, which are considerably lower than those found in
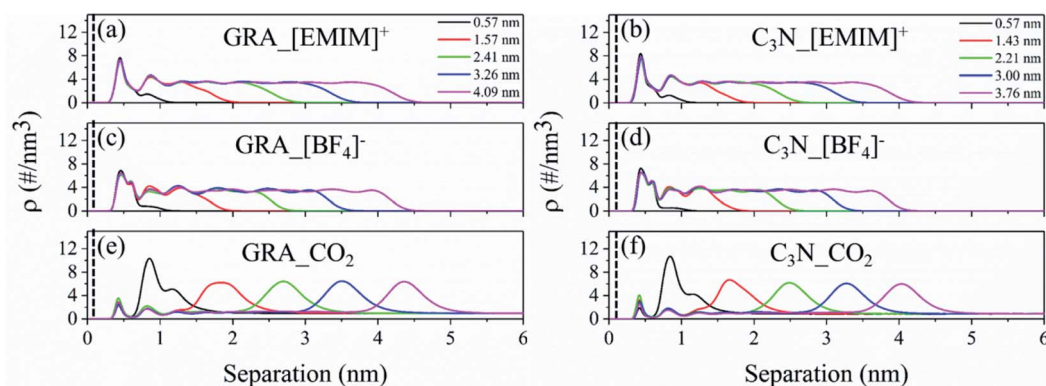

Fig. 2 Number density profiles of different compositions. (a and b) Represent the number density profiles of cations; (c and d) represent the number density profiles of anions; (e and f) represent the number density profiles of CO_2 molecules in the C_3N and GRA systems.

the two interfacial regions, independent of the variation of the IL film thickness. Fig. 3a depicts the total number of captured CO_2 with respect to the thickness of IL film. In the studied thickness region, roughly a linear dependency is found for both the GRA and C_3N systems. This is because when the IL film thickness increases, more CO_2 can be stored inside. However, when the CO_2 storage is normalized by the number of IL molecules (storage efficiency of the IL), which is depicted in Fig. 3b, the CO_2 storage efficiency increases quickly with the decrease in IL thickness, which is well consistent with SILM experimental reports.[31] These results are expected because a high-density layer of CO_2 is formed at the 0.7–1.1 nm from the substrates (Fig. 2e and f) where the IL density becomes considerably low (Fig. 2a–d). From these results, it is also deduced that the bulk IL region has lower CO_2 storage capability than two interfacial regions.

From the above-mentioned results, the role of two substrates is highlighted in the introduction of the two interfacial regions, which are rather attractive to CO_2 than to bulk IL. To quantitatively distinguish the roles of interfacial regions in attracting CO_2, we classified the captured CO_2 according to their locations, in detail: the substrate-IL interfacial region, the IL bulk and the IL-gas interfacial regions. As summarized in Table S1† (GRA systems) and Table S2† (C_3N systems), CO_2 residing inside the two interfacial regions are relatively constant despite the IL film thickness. More importantly, the IL-gas interface plays a more dominating role in the CO_2 storage than does the solid-IL interface. For the bulk IL region, the CO_2 storage efficiency is also considerably lower than that of the IL-gas interface.

In addition, no significant differences were detected between the GRA and C_3N systems. This is because the regulation of the substrate to the IL structure is short-ranged, which is limited to the solid-IL interface, and the contribution of the solid-IL interface in CO_2 storage is rather small. This is consistent with the previous report on using hydrophilic TiO_2 as SILM[14] where the CO_2 storage in the substrate-IL interfacial region was found to be small. Taken together, these results suggest that the capability of SILM is not sensitive to the specific type of supporting materials, which are mainly treated as substrates in the SILMs instead of amplifiers for the CO_2 capture.

3.3 Thin IL film facilitates quick CO_2 diffusion

Except for the gas capture process, the CO_2 mass transfer in the IL film is another determinative factor to evaluate the performance of the medium because a high rate of mass transfer is typically required. In addition, we studied the diffusion character of CO_2 molecules in the IL film. Technically, the mean square displacement (MSD) of CO_2 molecules along the transverse direction of the IL film was calculated. Then, the lateral diffusion coefficient (D) was fitted based on Einstein's relation $D = \lim_{t \to \infty} \frac{1}{4t} \langle [r_i(t) - r_i(0)]^2 \rangle$, where t is the time, and $r_i(t)$ and $r_i(0)$ are the positions of CO_2 i at time t and time 0, respectively.

Fig. 4a presents the specific values of D of the dissolved CO_2 in the GRA and C_3N systems with different IL film thicknesses. It is found that the diffusion of the dissolved CO_2 in both systems shows a decreasing trend with the increase in the IL thickness. According to the diffusion-reaction theory,[13] the bulk IL region was deduced to act as major resistance for the CO_2 diffusion. A thinner IL film can enhance the CO_2 diffusion. Accordingly, it is notable that there is a clear increase in the CO_2 diffusion at the IL thickness of 0.57 nm where the bulk IL region totally vanishes. These results suggest that the introduction of the interfacial IL regions by substrates greatly facilities the CO_2 diffusion. This is consistent with previous experimental reports that CO_2 exhibits faster kinetics in IL with substrates than that in pure IL.[11,32,33]

As in the IL medium, the diffusion of CO_2 is highly related to the cations and anions. We calculated the lateral diffusion coefficients of the cations and anions in both the GRA and C_3N systems (Fig. 4b) and found a similar vertiginous decrease tendency with the IL film thickness. Shi *et al.* reported that ions in IL diffuse faster with confinement from nano-materials at room temperature.[15] In our simulations, the confinement rate of IL by nano-sheets decreases with the IL film thickness, thus
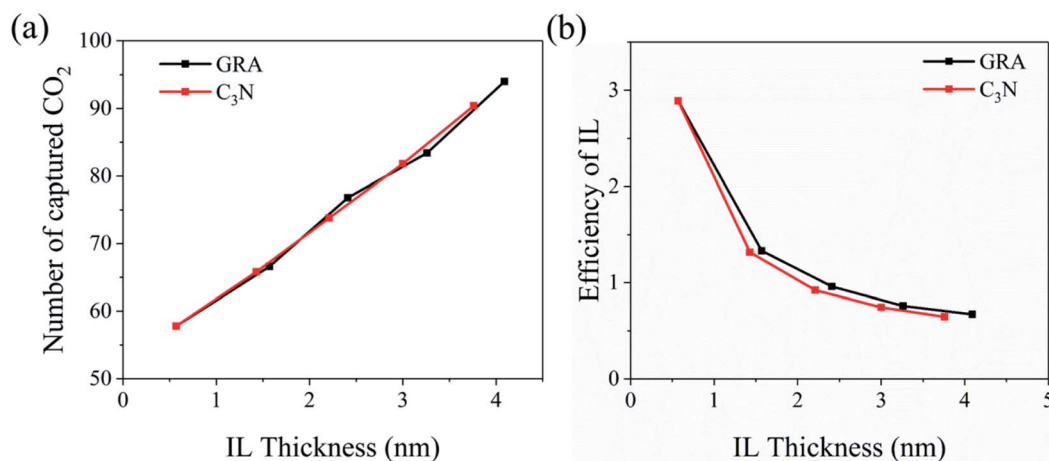

Fig. 3 (a) Total number of captured CO_2 with respect to IL thickness; (b) the CO_2 capture efficiency of the IL films with different thicknesses calculated by dividing the number of captured CO_2 by the total number of IL molecules.
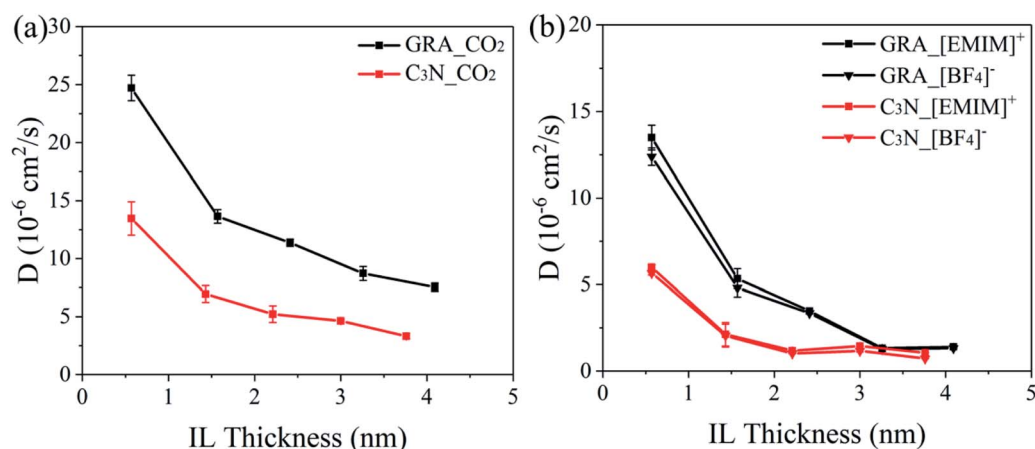
Fig. 4 Self-diffusion coefficients of the dissolved CO_2 molecules (a) and IL ions (b).

the ion diffusion is the fastest in the systems with the smallest IL film thickness. Additionally, the diffusion coefficients of ions in the C_3N systems are found comprehensively lower than those in the GRA systems. This is attributed to the stronger surface-IL interactions, which slow down the self-diffusion of ions, as reported by Shi *et al.*[15] We calculated the interaction energy of one ion binding onto GRA (-48.34 ± 11.24 kJ mol^{-1} for [EMIM]$^+$ and -13.53 ± 3.82 kJ mol^{-1} for [BF$_4$]$^-$) and C_3N (-49.02 ± 10.55 kJ mol^{-1} for [EMIM]$^+$ and -14.76 ± 3.32 kJ mol^{-1} for [BF$_4$]$^-$). For both the cation and anion, their interactions with C_3N are slightly higher than those with GRA. This explains the slower ion diffusion in the C_3N systems than that in the GRA systems.

3.4 Quantitative interpreting CO_2-binding affinity and structural mechanisms

To gain a deep understanding of the binding behavior of CO_2 inside the IL film, the binding affinity changes of a CO_2 molecule translocating from the gas region into the IL interior is studied by calculating the potential of mean force (PMF) by the umbrella-sampling method. As summarized in Fig. 5, the PMF profiles illustrate that the global minimum, around -6 kJ mol^{-1}, is located at the IL-gas interface in both GRA and C_3N systems, which is well consistent with the CO_2 distribution shown in Fig. 2c and f. In addition, there are two local minima near the two nanosheets, corresponding to the two density peaks of CO_2 at the solid-IL interface in Fig. 2c and f. These minima, particularly those at the IL-gas interface, reflect the strong attraction of interfacial regions to CO_2 molecules and the accumulation of CO_2. In the bulk IL, the PMF profiles are relatively flat and generally higher than those at the IL-gas interface, corresponding to the overall CO_2 storage capability of IL itself.

To probe the atomic mechanism of such patterned CO_2 distribution inside the IL film, we further accessed the microscopic structure of the molecule assembly in the IL film by calculating the orientations of the [EMIM]$^+$ cations and CO_2. The [BF$_4$]$^-$ anions were ignored because of their tetrahedron shapes. We defined two tilt angles for [EMIM]$^+$ to describe the orientation of the cation: one is the angle between the ethyl
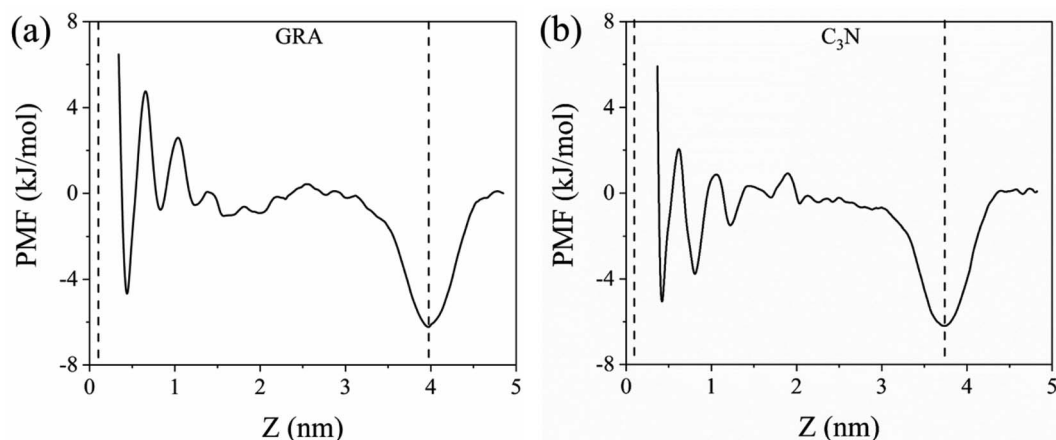

Fig. 5 Potential of mean force (PMF) for CO_2 diffusion from the IL-gas interface to the substrate-IL interface. The dashed lines represent the position of the two interfaces.

chain and the normal direction of the substrate (Fig. 6a); the other is the dihedral angle between the imidazole ring plane and the substrate (Fig. 6e). The orientation of the CO_2 molecule is described by the angle between the linear CO_2 and the normal direction of the substrate (Fig. 6i).

We used the GRA system as a representative for discussions, and three IL films with thicknesses of 0.57, 2.41 and 4.09 nm were compared, as shown in Fig. 6. The corresponding results for the C_3N system are generally similar, as shown in Fig. S2 in ESI.† In a thin IL film, orientations of the cations are strongly influenced by the nanosurface. The orientations of the IL cations and CO_2 are highly biased at the substrate-IL and IL-gas regions. From the angle distributions, we observed two distinguishable spots for the ethyl chain tilt angle (Fig. 6b), which are labelled as s1 (around 50°) and s2 (90°), respectively. Two indistinguishable spots for the imidazole ring tilt angle (Fig. 6f), which are both labelled s3 (at equivalent 0° and 180°), can also be detected. From this information, it is seen that the cations stack to the substrate with the imidazole ring parallels to the substrate surface. However, for the ethyl chains, they are flexible enough to be alternatively attached to or detached from the surface, as illustrated by the two representative structures embedded in Fig. 6b. In addition, the CO_2 molecules at the substrate-IL interfacial region adopt a parallel binding pose to the nanosurface (as shown in Fig. 6j) because the tilt angle is located at around 90° (Fig. 6j, s4). Such a binding mode maximizes the intimate contacts between CO_2 and the substrates, representing the stronger attraction from the nano-surface than from IL.

It is notable that the three tilt angles are highly conserved in the substrate-IL interfacial region, regardless of the IL thickness. This is also true for the tilt angles of the ethyl chains, which are restrained between 30° and 60° (Fig. 6c and d, s5), indicating that the ethyl chains of $[EMIM]^+$ point to the gas phase. This is in line with the finding that more ethyl groups are located at the IL-gas interfaces than at the imidazolium rings (Fig. S3†). Such structure is also consistent with previous experimental reports that, at the IL-gas interface, a longer alkyl chain of cations tends to point to the gas phase.[34] As for the CO_2 molecules at the IL-gas interface, a parallel orientation along the surface is also favored although the specific angle spreads in a range of 60–120° (Fig. 6j–l, s6). Such orientation also ensures intimate binding of CO_2 with IL.[35] In general, from these analyses, the assembled CO_2 in two interfacial regions are accompanied by the directionally-oriented CO_2 and cations, indicating structural compatibility among them.

From the above-mentioned analyses, the orientations of CO_2 in IL are highly regulated by the two interfacial regions. In addition, the dynamic characteristics of the CO_2 molecules in the two interfacial regions are also different, as revealed by the residence time of CO_2 (Fig. S4†). The CO_2 residence time at the IL-gas interface distributes mainly around 40–50 ps in both GRA systems and C_3N systems, which indicates the stable CO_2 adsorption at the IL-gas interfaces. In contrast, the residence time at the substrate-IL interface is more dispersed than that at the IL-gas interface (Fig. S4†). It is found that the binding at the substrate-IL interface can either last for more than 100 ps (mainly representing CO_2 molecules in the first adsorption layer
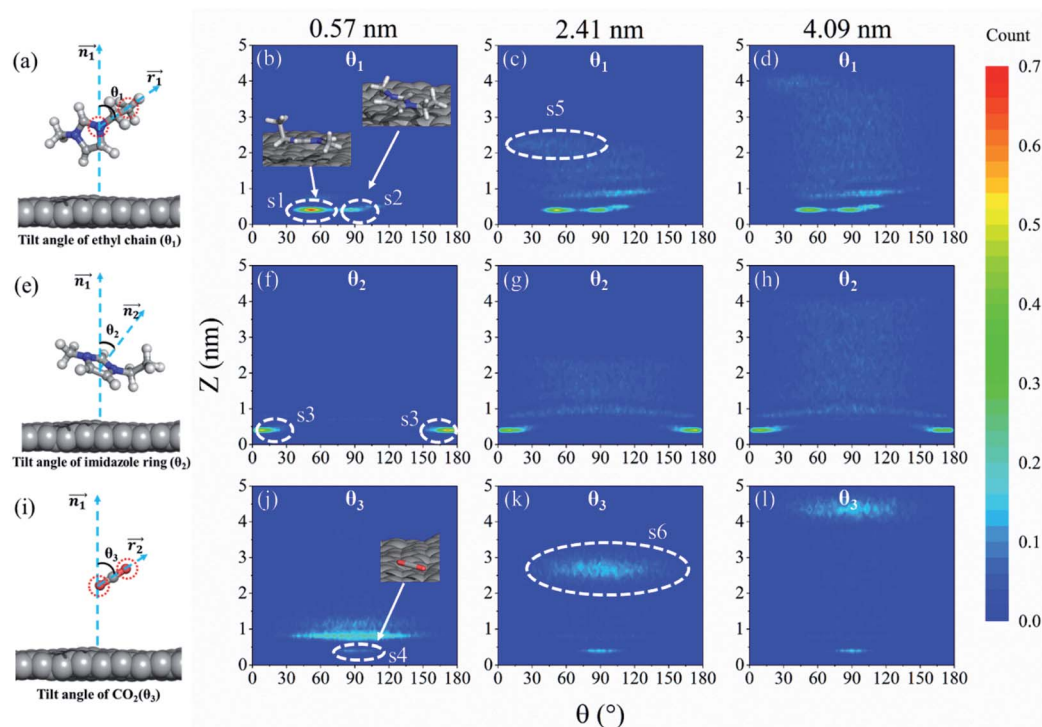

Fig. 6 Definition and distribution of the tilt angles of the ethyl side chain of cations (a–d), imidazolium ring of cations (e–h) and CO_2 (i–l) in three IL films attached to GRA with the IL thickness of 0.57 nm, 2.41 nm and 4.09 nm, respectively.

of the substrate-IL interface) or less than 10 ps, which represent CO_2 molecules that cannot form a significant residence in the IL-gas interface region.

4. Conclusion

Using all atomic molecular dynamics simulations, we studied the structural and energetic characteristics of SILM with CO_2 capture. By coating different number of [EMIM][BF$_4$] pairs onto the nanosheet, the influences of the IL film thickness are systematically discussed. First, the CO_2 accumulation at the IL-gas interfacial region dominates the CO_2 capture by SILM, suggesting the minor role of specific substrate materials. In general, the CO_2 capturing efficiency of supported IL increases with a decrease in the IL film thickness. A sub-nanometer IL film possesses the highest CO_2 capture efficiency because of the formation of a reduced bulk IL region. The nanomaterial surfaces can effectively accelerate the diffusion of CO_2, which is beneficial for the CO_2 mass transfer. The current study provides deep understanding of the molecular interactions at the interfaces of SILMs, and paves the way for the design and fabrication of optimized supporting nanomaterials of SILM for the CCS usage.

Conflicts of interest

There are no conflicts to declare.

Acknowledgements

References

1 A. E. Creamer and B. Gao, *Environ. Sci. Technol.*, 2016, **50**, 7276–7289.

2 M.-O. Schach, R. d. Schneider, H. Schramm and J.-U. Repke, *Ind. Eng. Chem. Res.*, 2010, **49**, 2363–2370.

3 L. A. Blanchard, D. Hancu, E. J. Beckman and J. F. Brennecke, *Nature*, 1999, **399**, 28–29.

4 M. Aghaie, N. Rezaei and S. Zendehboudi, *Renewable Sustainable Energy Rev.*, 2018, **96**, 502–525.

5 M. J. Earle, J. M. Esperanca, M. A. Gilea, J. N. Lopes, L. P. Rebelo, J. W. Magee, K. R. Seddon and J. A. Widegren, *Nature*, 2006, **439**, 831–834.

6 M. Kosmulski, J. Gustafsson and J. B. Rosenholm, *Thermochim. Acta*, 2004, **412**, 47–53.

7 M. Bui, C. S. Adjiman, A. Bardow, E. J. Anthony, A. Boston, S. Brown, P. S. Fennell, S. Fuss, A. Galindo, L. A. Hackett, J. P. Hallett, H. J. Herzog, G. Jackson, J. Kemper, S. Krevor, G. C. Maitland, M. Matuszewski, I. S. Metcalfe, C. Petit, G. Puxty, J. Reimer, D. M. Reiner, E. S. Rubin, S. A. Scott, N. Shah, B. Smit, J. P. M. Trusler, P. Webley, J. Wilcox and N. Mac Dowell, *Energy Environ. Sci.*, 2018, **11**, 1062–1176.

8 X. Liu, G. Zhou, S. Zhang and X. Yao, *Fluid Phase Equilib.*, 2009, **284**, 44–49.

9 B. F. Goodrich, J. C. de la Fuente, B. E. Gurkan, D. J. Zadigian, E. A. Price, Y. Huang and J. F. Brennecke, *Ind. Eng. Chem. Res.*, 2011, **50**, 111–118.

10 R. D. Noble and D. L. Gin, *J. Membr. Sci.*, 2011, **369**, 1–4.

11 X. Wang, N. G. Akhmedov, Y. Duan, D. Luebke and B. Li, *J. Mater. Chem. A*, 2013, **1**, 2978–2982.

12 W. Xie, X. Ji, X. Feng and X. Lu, *Ind. Eng. Chem. Res.*, 2015, **55**, 366–372.

13 W. Xie, X. Ji, X. Feng and X. Lu, *AIChE J.*, 2015, **61**, 4437–4444.

14 Z. Tang, L. Lu, Z. Dai, W. Xie, L. Shi and X. Lu, *Langmuir*, 2017, **33**, 11658–11669.

15 W. Shi and D. R. Luebke, *Langmuir*, 2013, **29**, 5563–5572.

16 S. Yang, W. Li, C. Ye, G. Wang, H. Tian, C. Zhu, P. He, G. Ding, X. Xie, Y. Liu, Y. Lifshitz, S. T. Lee, Z. Kang and M. Jiang, *Adv. Mater.*, 2017, **29**, 1605625.

17 X. Li, T. Guo, L. Zhu, C. Ling, Q. Xue and W. Xing, *Chem. Eng. J.*, 2018, **338**, 92–98.

18 G. Qin, Q. Cui, W. Wang, P. Li, A. Du and Q. Sun, *Chemphyschem*, 2018, **19**, 2788–2795.

19 X. Li, Y. Yin, X. Chang, Y. Xiong, L. Zhu, W. Xing and Q. Xue, *Chem. Eng. J.*, 2020, **387**, 123403.

20 J. Rafiee, X. Mi, H. Gullapalli, A. V. Thomas, F. Yavari, Y. Shi, P. M. Ajayan and N. A. Koratkar, *Nat. Mater.*, 2012, **11**, 217–222.

21 M. J. Abraham, T. Murtola, R. Schulz, S. Páll, J. C. Smith, B. Hess and E. Lindahl, *SoftwareX*, 2015, **1–2**, 19–25.

22 V. V. Chaban, I. V. Voroshylova and O. N. Kalugin, *Phys. Chem. Chem. Phys.*, 2011, **13**, 7910–7920.

23 Y. Deng, F. Wang, Y. Liu, Y. Yang, Y. Qu, M. Zhao, Y. Mu and W. Li, *Nanoscale*, 2020, **12**, 5217–5226.

24 B. Hess, H. Bekker, H. J. C. Berendsen and J. G. E. M. Fraaije, *J. Comput. Chem.*, 1997, **18**, 1463–1472.

25 U. Essmann, L. Perera, M. L. Berkowitz, T. Darden, H. Lee and L. G. Pedersen, *J. Chem. Phys.*, 1995, **103**, 8577–8593.

26 G. Bussi, D. Donadio and M. Parrinello, *J. Chem. Phys.*, 2007, **126**, 014101.

27 G. M. Torrie and J. P. Valleau, *J. Comput. Phys.*, 1977, **23**, 187–199.

28 S. Kumar, J. M. Rosenberg, D. Bouzida, R. H. Swendsen and P. A. Kollman, *J. Comput. Chem.*, 1995, **16**, 1339–1350.

29 B. Roux, *Comput. Phys. Commun.*, 1995, **91**, 275–282.

30 M. Atilhan and S. Aparicio, *J. Phys. Chem. C*, 2018, **122**, 1645–1656.

31 N. Wu, X. Ji, W. Xie, C. Liu, X. Feng and X. Lu, *Langmuir*, 2017, **33**, 11719–11726.

32 P. Fan, X. Qiu, F. U. Shah, Q. Ji and R. An, *Phys. Chem. Chem. Phys.*, 2020, **22**, 1097–1106.

33 X. Wang, N. G. Akhmedov, Y. Duan, D. Luebke, D. Hopkinson and B. Li, *ACS Appl. Mater. Interfaces*, 2013, **5**, 8670–8677.

34 S. Rivera-Rubero and S. Baldelli, *J. Phys. Chem. B*, 2006, **110**, 4756–4765.

35 M. E. Perez-Blanco and E. J. Maginn, *J. Phys. Chem. B*, 2010, **114**, 11827–11837.